

CrystEngComm

Accepted Manuscript



This is an *Accepted Manuscript*, which has been through the Royal Society of Chemistry peer review process and has been accepted for publication.

Accepted Manuscripts are published online shortly after acceptance, before technical editing, formatting and proof reading. Using this free service, authors can make their results available to the community, in citable form, before we publish the edited article. We will replace this *Accepted Manuscript* with the edited and formatted *Advance Article* as soon as it is available.

You can find more information about *Accepted Manuscripts* in the [Information for Authors](#).

Please note that technical editing may introduce minor changes to the text and/or graphics, which may alter content. The journal's standard [Terms & Conditions](#) and the [Ethical guidelines](#) still apply. In no event shall the Royal Society of Chemistry be held responsible for any errors or omissions in this *Accepted Manuscript* or any consequences arising from the use of any information it contains.

Cite this: DOI: 10.1039/c0xx00000x

www.rsc.org/crystengcomm

ARTICLE TYPE

The Influence of 1-alkyl-3-methyl Imidazolium Ionic Liquids on A Series of Cobalt-1,4-benzenedicarboxylate Metal-organic Frameworks

Ling Xu^{a,*}, Bing Liu^b, Sheng-Xian Liu^a, Huan Jiao^a, Luís Cunha-Silva^{c,*}

Received (in XXX, XXX) Xth XXXXXXXXXX 20XX, Accepted Xth XXXXXXXXXX 20XX

DOI: 10.1039/b000000x

To investigate the influence of ionic liquids on the structures and the properties of the complexes, ionothermal synthesis of 1,4-benzenedicarboxylate acid (H₂BDC) reacting with Co(NO₃)₂ under four 1-alkyl-3-methylimidazolium bromide produced three layered metal-organic frameworks with chemical formula [RMI]₂[Co₃(BDC)₃Br₂], (R = ethyl for **1**; n-propyl for **2**, and n-butyl for **3**; MI = imidazolium) and 3D architecture [AMI]₂[Co₃(BDC)₄] (**4**) (A = amyl). Compounds **1-3** have the same (3,6) skeleton with [RMI]⁺ cations locating in the interlayer space. Compound **4** grows into a 3D architecture based on BDC²⁻ ligands linking the similar 2D grids as those in **1-3**. The [RMI]⁺ templates exert their influence on the diagonal sizes of the quadrilateral grids, the interlamellar spacing, and the solvent-accessible cavities through steric hindrances. By the comparison of **1-3**, the [RMI]⁺ templates also find the roles on the properties. With the alkyl chains in [RMI]⁺ increasing, the decomposing temperatures increase, emission peaks around 400 nm blue shift, and the cavities of **1-3** decrease. The magnetic behaviors of **1-3** are ferromagnetism with similar magnetic parameters, while **4** reveals antiferromagnetism.

Introduction

Ionothermal synthesis as an environment-friendly method has received remarkable attention in the latest decade,^{1,2,3} in which ionic liquids (ILs) behave as reaction media, structural templates or charge-compensating groups.^{4,5} ILs have many distinguishing features: high ionic conductivity, non-flammability, negligible vapor pressure, and so forth,^{6,7} contributing for new-type meso- and macroporous materials, and metal-organic frameworks (MOFs).^{8,9} MOFs are a kind of porous materials with significance applications in gas storage, catalysis, and electronic chemistry.^{10,11} With the consideration of the difference between ILs and the common organic solvents/water, ionothermal method is reasonably expected to offer significantly different reaction environments to produce new-type MOF materials. Enormous effort has been devoted to the applied ionothermal synthesis of novel MOF materials.^{12,13,14} Besides the selection of ligands and metal centers, the components of ILs play critical roles in the structural fabrications of MOFs: cationic parts usually act as prime structure templates locating in the cavities; while anionic parts affect the deprotonated degree of the ligands through their hydrophilicity/hydrophobicity or nucleophilicity/basicity behaviors.

Our previous work on M-BTC systems (M = Zn, Cd, Ni; H₃BTC = benzene-1,3,5-tricarboxylic acid) deduced the aforementioned ILs' roles, in which the effects of metal-direction, cationic template, anionic groups on the MOFs' structures can be distinctly observed.¹⁵ It becomes an important strategy in

achieving novel MOF materials through tuning the properties of ILs through tailoring the alkyl chains or the anion types, and then transmitting the effects to the structural constructions of MOFs, thus controlledly synthesizing MOF materials with desired properties. Our present work aims at the so-called "ionic liquid effect".² To watch more clearly how the ILs work on the properties of MOFs, we hope to eliminate the effects of metal centers and ligands. Therefore, we fix 1,4-benzenedicarboxylate acid (H₂BDC) as ligand with simpler coordination fashions, and Co(NO₃)₂ as metal source to obtain MOFs with similar/same skeletons, thus to recognize the ionic liquid effect. H₂BDC reacted with Co(NO₃)₂ at different ratios under ionothermal conditions using four kinds of ILs as reaction media: 1-ethyl-3-methylimidazolium bromide ([EMI]Br), 1-propyl-3-methylimidazolium bromide ([PMI]Br), 1-butyl-3-methylimidazolium bromide ([BMI]Br), 1-amyl-3-methylimidazolium bromide ([AMI]Br). Three similar 2D MOFs formulated as [RMI]₂[Co₃(BDC)₃Br₂] (RMI = [EMI]⁺ for **1**; [PMI]⁺ for **2**, and [BMI]⁺ for **3**), and one 3D MOF architecture [AMI]₂[Co₃(BDC)₄] (**4**) are presented in this work. The ionic liquid effect on the structures and the properties of TG, fluorescence, magnetism are clearly observed.

Experimental Section

Materials and physical measurements. The reagents and solvents were used directly as supplied commercially without further purification except four kinds of 1-alkyl-3-methylimidazolium bromide synthesized from the reaction of 1-

alkyl bromide with 1-methylimidazole according to literature processes.¹⁶ Degassed alkylbromide were refluxed with the distilled 1-methylimidazole to give corresponding ILs. The four sorts of ILs were washed with ethyl acetate, and then dried under a vacuum at least for 10 h: [EMI]Br (white solid, m.p. = 80–82 °C, yield: 92%), [PMI]Br (pale yellow oil, yield: 80%), [BMI]Br (pale yellow oil, yield: 78%), [AMI]Br (pale brown oil, yield: 68%).

FT-IR spectra were collected from KBr pellets (Aldrich, >99%, FT-IR grade) with a Bruker Tensor 27 FT-IR spectrometer in the range of 4000–400 cm⁻¹. Thermogravimetric (TG) analyses were carried out in N₂ atmosphere on a SDT Q600 V8.3 Build 101 instrument with a heating rate of 10 °C·min⁻¹ and a N₂ flow rate of 20 cm³·min⁻¹. Powder X-ray diffraction data for the materials were collected at ambient temperature with a Rigaku D/Max-3c (Japan) diffractometer (Cu-Kα_{1,2} X-radiation, λ₁ = 1.540598 Å and λ₂ = 1.544426 Å), equipped with an X'Celerator detector and a flatplate sample holder in a Bragg–Brentano para-focusing optics configuration (40 kV, 50 mA). Intensity data were collected by the step counting method (step being 0.02°), in continuous mode, in the ca. 5 ≤ 2θ ≤ 50° range. Magnetic susceptibilities were measured with a quantum Design MPMS-XL-7 SQUID magnetometer in the temperature range 2.0–300.0 K with the applied magnetic field was 1000 Oe.

Synthesis of [EMI]₂[Co₃(BDC)₃Br₂], 1. 1.00 mmol, 0.2919 g Co(NO₃)₂·6H₂O and 0.50 mmol, 0.0831 g H₂BDC were placed in a crystallisation vial placed in a 25 mL Teflon-lined stainless-steel autoclave mixed with 1.005 g [EMI]Br. The mixture was kept inside the furnace at 140 °C for 7 days, and then naturally cooled to ambient temperature. The blue crystals of **1** suitable for X-ray diffraction were collected after soak clearing with acetone. IR data (in KBr, cm⁻¹) for **1**: 3419(m), 3145(w), 3105(w), 3079(w), 2991(w), 2934(w), 1627(s), 1596(s), 1504(m), 1380(s), 1301(s), 1165(m), 1130(m), 1015(m), 899(w), 817(m), 746(s), 656(w), 612(w), 548(m). Compound **1** can be also synthesized by 0.50 mmol, 0.1469 g Co(NO₃)₂·6H₂O and 0.50 mmol, 0.0835 g H₂BDC mixed with 1.003 g [EMI]Br in the same way, or with the same amount of raw materials at 160 °C under similar process.

Synthesis of [PMI]₂[Co₃(BDC)₃Br₂], 2. Compound **2** can be synthesized from the similar preparation process as described in compound **1** by using 1.00 mmol, 0.2913 g Co(NO₃)₂·6H₂O and 0.50 mmol, 0.0838 g H₂BDC mixed with 1.0 ml [PMI]Br. IR data (in KBr, cm⁻¹) for **2**: 3419(m), 3145(m), 3088(m), 2960(w), 2925(m), 2868(m), 2758(w), 2679(w), 2635(w), 2578(w), 2516(w), 2428(w), 1961(w), 1838(w), 1614(s), 1581(s), 1504(m), 1380(s), 1297(s), 1161(m), 1130(m), 1007(m), 890(w), 820(s), 744(s), 649(w), 619(w), 548(m). Compound **2** can be also achieved by 1.50 mmol, 0.4370 g Co(NO₃)₂·6H₂O and 0.50 mmol, 0.0838 g H₂BDC mixed with 1.0 ml [PMI]Br through the similar process as that of compound **1**, or with the same amount of raw materials at 160 °C.

Synthesis of [BMI]₂[Co₃(BDC)₃Br₂], 3. Prepared as described in **1**, compound **3** was obtained from the mixture of 1.00 mmol, 0.2915 g Co(NO₃)₂·6H₂O, and 0.50 mmol, 0.0835 g H₂BDC with 1.0 ml [BMI]Br. IR data (in KBr, cm⁻¹) for **3**: 3428(s), 3141(m), 3106(m), 3080(m), 2987(m), 2930(w), 2870(w), 2849(w), 2803(w), 2761(w), 2575(w), 2521(w), 2422(w), 1625(s), 1584(s), 1508(m), 1387(s), 1330(s), 1304(s), 1161(s), 1130(s), 1087(w),

1016(m), 890(w), 820(s), 749(s), 652(w), 613(w), 575(w), 553(s). Compound **3** can be synthesized with the same amount of raw materials at 160 °C under similar process.

Synthesis of [AMI]₂[Co₃(BDC)₄], 4. With the similar preparation process of **1**, the mixture of 1.00 mmol, 0.2911 g Co(NO₃)₂·6H₂O and 0.50 mmol, 0.0837 g H₂BDC with 1.0 ml [AMI]Br gave compound **4**. IR data (in KBr, cm⁻¹) for **4**: 3707(w), 3603(w), 3541(s), 3335(s), 3273(s), 3215(s), 3162(s), 3106(s), 3048(s), 2978(w), 2934(w), 2886(w), 2828(w), 2771(w), 2714(w), 2657(w), 2556(w), 1868(w), 1799(w), 1635(m), 1508(w), 1455(w), 1380(w), 1097(s), 1047(s), 917(w), 791(s), 693(w), 628(m), 481(s).

Topology. According to A. F. Wells' topology definition¹⁷ and the MOF structural features, the constructed secondary building units (SBUs) and the rest benzene ring from BDC²⁻ ligand are simplified as the nodes and the topology networks of compounds **1-4** were calculated using the ADS program of the TOPOS 4.0 Professional structure-topological program package.¹⁸

Single Crystal X-ray Diffraction. Single crystals of compounds **1-4** were manually harvested from crystallisation vials and mounted on Hampton Research CryoLoops using FOMBLIN Y perfluoropolyether vacuum oil (LVAC 25/6, purchased from Aldrich)¹⁹ with the help of a Stemi 2000 stereomicroscope equipped with Carl Zeiss lenses. Data were collected with a Bruker X8 Kappa APEX II charge-coupled device (CCD) area-detector diffractometer (Mo-Kα graphite-monochromated radiation, λ = 0.71073 Å) controlled by the APEX2 software package,²⁰ and equipped with an Oxford Cryosystems Series 700 cryostream monitored remotely using Cryopad²¹ at 150(2) K. Images were processed using SAINT+,²² and data were corrected for absorption by the multiscan semiempirical method implemented in SADABS.²³

The structures of compounds **1-4** were solved by direct methods using SHELXTLTM package of crystallographic software²⁴ and refined by full-matrix least-squares technique on F². All non-hydrogen atoms were refined anisotropically. Hydrogen atoms were located at geometrically calculated positions to their carrier atoms and refined with isotropic thermal parameters included in the final stage of the refinement. A summary of the structural determination and refinement for **1-4** is listed in Table 1. The selected bond distance and angles are listed in Supporting Information (Supporting Information, Table S1).

Crystallographic data (excluding structure factors) for the structures reported in this paper have been deposited with the Cambridge Crystallographic Data Centre (the deposition numbers CCDC 1006451–1006454 for **1-4** respectively). These data can be obtained free of charge from The Cambridge Crystallographic Data Centre via www.ccdc.cam.ac.uk/data_request/cif.

Table 1. Crystal and structure refinement data for compounds **1-4**

	1	2	3	4
Empirical formula	C ₃₆ H ₃₄ Br ₂ Co ₃ N ₄ O	C ₃₈ H ₃₈ Br ₂ C ₃ N ₄ O ₁₂	C ₄₀ H ₄₂ Br ₂ C ₃ N ₄ O ₁₂	C ₅₀ H ₅₀ Co ₃ N ₄ O ₁₆
Color and Habit	blue prism	violet prism	violet prism	violet prism
Crystal Size (mm ³)	0.120×0.120×0.030	0.12×0.09×0.06	0.18×0.10×0.06	0.18×0.13×0.05

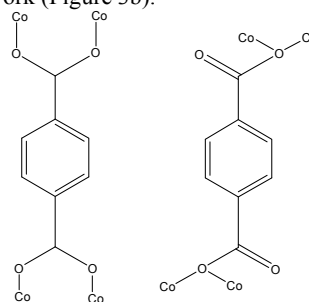
Crystal system	Monoclinic	Monoclinic	Monoclinic	Monoclinic
Space group	$P2_1/n$	$P2_1/n$	$P2_1/n$	$C2/c$
a (Å)	12.9273(11)	12.9773(6)	13.0822(12)	33.093(3)
b (Å)	9.3874(9)	9.4496(4)	9.7472(8)	9.6403(9)
c (Å)	18.2110(16)	18.2310(9)	18.0158(16)	18.5130(19)
β (°)	107.861(4)	108.237(2)	108.963(3)	92.954(5)
V (Å ³)	2103.5(3)	2123.37(17)	2172.6(3)	5898.3(10)
Z	2	2	2	4
F_w	1051.28	1079.33	1107.39	1139.73
D_c (Mgm ⁻³)	1.660	1.688	1.693	1.283
μ (mm ⁻¹)	3.131	3.104	3.036	0.898
$F(000)$	1050	1082	1114	2348
θ (°)	3.40 to 25.03	3.81 to 27.48	3.75 to 27.48	3.70 to 25.02
Reflections measured	14181	33494	18735	20895
Independent refs	3644 ($R_{int} = 0.0739$)	4865 ($R_{int} = 0.0570$)	4969 ($R_{int} = 0.0594$)	5131 ($R_{int} = 0.0484$)
Observed Refs	2262	3999	3376	3504
$[I > 2\sigma(I)]$				
Final R_1, wR_2	0.0774, 0.1950	0.0321, 0.0742	0.0474, 0.0994	0.0680, 0.1929
$[I > 2\sigma(I)]$				
R_1, wR_2 (all data)	0.1120, 0.2066	0.0458, 0.0822	0.0849, 0.1142	0.0939, 0.2061
S	1.006	0.952	1.060	1.007
$(\Delta/\sigma)_{max/min}$	0.004, 0.000	0.001, 0.000	0.001, 0.000	0.001, 0.000
$\Delta\rho_{max/min}$ (eÅ ⁻³)	2.828, -0.730	1.112, -0.808	1.143, -0.718	1.305, -0.463

$$R_1 = (\sum |F_o| - |F_c|) / \sum |F_o|. wR_2 = [\sum (w(F_o^2 - F_c^2)^2) / \sum (w|F_o^2|)]^{1/2}$$

Results and discussion

Crystal structures of compounds 1-3. 2D layered compounds **1-3**, $[RMI]_2[Co_3(BDC)_3Br_2]$, possess same $[Co_3(BDC)_3Br_2]$ skeleton frameworks with corresponding $[RMI]^+$ cations anchoring in the interlayer spaces, including the same coordination spheres of Co(II) centers and the coordination fashions of BDC^{2-} ligands. Because of the skeleton framework similarity in compounds **1-3**, only the structure of compound **1** will be discussed in detail. The structural motifs of compounds **2** and **3** are listed in supplementary information (Supporting Information, Figure S1-5). The asymmetric unit of compound **1** consists of one and half Co(II) centers, one and half BDC^{2-} ligands, one Br^- and one $[EMI]^+$ (Figure 1). Four positive charges on Co(II) centers and $[EMI]^+$ cation are neutralized by one and half BDC^{2-} ligands and one Br^- to keep charge balance. In compound **1**, BDC^{2-} ligands exhibit two μ_4 coordination modes: bis-bidentate and bridging monodentate coordination fashions (Scheme 1). Two independent Co1 and Co2 centers have different coordination geometries. A distorted tetrahedron

coordination sphere of Co1 center is shaped by three carboxylic oxygen atoms and one terminal monodentate Br^- ligand with $d_{Co1-O} = 1.963(3) - 1.982(3)$ Å and $d_{Co1-Br} = 2.394(9)$ Å, respectively. Co2 center bonding with six carboxylic oxygen atoms builds into a distorted octahedron, in which four carboxylic oxygen atoms are placed in the equatorial plane, and O21 and its symmetric atom locate in the axial vertices. Co2 center links each Co1 center through two pairs of μ_2 -bidentate COO^- groups and one μ_2 -bridging monodentate COO^- group. Consequently, Co2 center as a central symmetric point connects Co1 center and its symmetric atom into a linear trinuclear $[Co_3(COO)_6Br_2]$ SBU with Co...Co interactions of 3.236 Å (Figure 2). Such four $[Co_3(COO)_6Br_2]$ SBUs are further bridged by four rest benzene moieties from BDC^{2-} ligands of μ_4 -bis-bidentate mode into a 36-membered quadrilateral, whose propagation produces a layered (4,4) sheet along the bc -plane (Supporting Information, Figure S6). The other kind of benzene moieties from BDC^{2-} ligands of μ_4 -bridging monodentate mode embed into the 36-membered quadrilateral along the b -direction (Supporting Information, Figure S7). Ultimately, a (3,6) topological layer constructed by dummied $[Co_3(COO)_6Br_2]$ SBUs and benzene rings as 6- and 2-connecting nodes (Figure 3c). The $[EMI]^+$ cations appear in the interlayer; however, no 3D supramolecular architecture can be built up based on no strong interaction among $[EMI]^+$ cations and the negative framework (Figure 3b).



Scheme 1. The coordination fashions of BDC^{2-} ligands in compounds **1-3**.

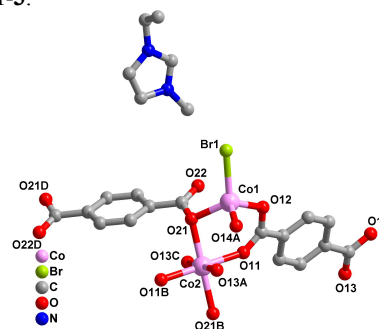


Figure 1. Coordination spheres of Co(II) centers in compound **1**.

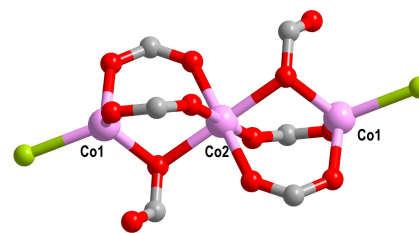


Figure 2. The structure motif of the linear trinuclear $[\text{Co}_3(\text{COO})_6\text{Br}_2]$ SBU in compound 1.

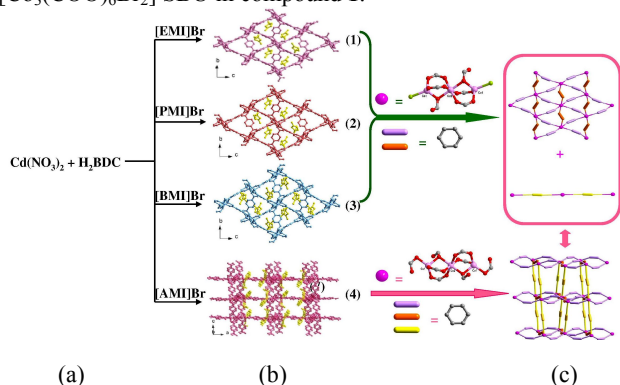
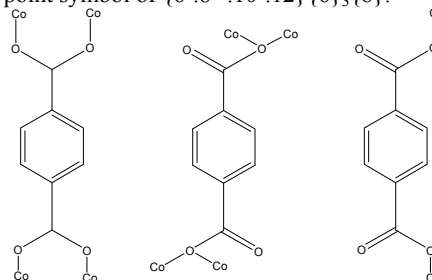


Figure 3. Schematic representation of (a) the reactions investigated; (b) the crystal structures, packing arrangements, with the ILs cations represented in yellow and the anionic 2D frameworks drawn in purple, pink, blue and amaranth, respectively; (c) the (3,6) 2D topological network for compounds 1-3 and 3D $\{6^6.8^{14}.10^7.12\}\{6\}_3\{8\}$ topological network for 4 with the trinuclear $[\text{Co}_3(\text{COO})_6\text{Br}_2]$ subunits for 1-3 considered as six-connected nodes, the $[\text{Co}_3(\text{COO})_8]$ subunit considered as eight-connected node for 4 and rest benzene moieties as two-connected nodes for 1-4.

Crystal structure of compound 4. Compound 4, $[\text{AMI}]_2[\text{Co}_3(\text{BDC})_4]$, distinguishes itself from compounds 1-3 in which 4 is a 3D architecture organized on the base of the 2D sheets in 1-3. The asymmetric unit of 4 contains one and half independent Co(II) centers, two BDC^{2-} ligands and one $[\text{AMI}]^+$ cation (Figure 4). Three positive charges on Co(II) centers and one on $[\text{AMI}]^+$ are balanced by two BDC^{2-} anions. Similarly, the independent Co1 and Co2 centers shape tetrahedral and octahedron geometries respectively, except that the Co1-Br bonds in 1-3 are replaced by Co1-O bonds. Additionally, the BDC^{2-} ligand exhibits three kinds of coordination fashions: μ_4 -bis-bidentate and μ_4 -bridging monodentate modes as that of compounds 1-3, and a different μ_2 bis-monodentate mode (Scheme 2). Co2 atom as a crystallographic inversion center connect Co1 and its symmetric atom building up a similar linear trinuclear negative $[\text{Co}_3(\text{COO})_8]$ SBU based on the similar connection ways, except a monodentate COO^- group as a terminal ligand replacing Br^- existing in Co1 sphere (Figure 5). Also, $[\text{Co}_3(\text{COO})_8]$ SBUs are connected by μ_4 -bis-bidentate BDC^{2-} ligands into a (4,4) sheet, and further by μ_4 -bridging monodentate BDC^{2-} ligands embedded in the 36-membered quadrilateral into a (3,6) topological layer along the *bc*-plane (Supporting Information, Figure S8). This construction ways of the (3,6) layers in compounds 1-4 are identical. Subsequently, these neighbouring (3,6) layers are fused into a 3D architecture based on the connection of μ_2 -bis-monodentate COO^- groups (Figure 3c). When omitting $[\text{AMI}]^+$, the total solvent-accessible volume of the channels in the unit is 3306.5 \AA^3 , which accounts for 56.1% of the total cell volume 5898.3 \AA^3 calculated by PLATON software;²⁵ Considering $[\text{AMI}]^+$ anchoring in the channels, the solvent-accessible volume significantly decreases to 1248.1 \AA^3 , accounting for 21.2%. The calculation indicates that, though $[\text{AMI}]^+$ templates block up nearly 60% cavities, there is

still 21.2% cavities existing in the framework. It relates with the arrangement of the $[\text{AMI}]^+$ templates, which economizes the space: $[\text{AMI}]^+$ template locating between the adjacent μ_2 bis-monodentate BDC^{2-} ligands and the orientations of BDC^{2-} ligands posing in the opposite direction (Figure 3b). We will have a better insight into the nature of this intricate architecture by topological analysis. Regarding on the structural features of 4, apparently, the $[\text{Co}_3(\text{COO})_8]$ SBUs could be regarded as 8-connected nodes, and the rest benzene moieties as 2-connected nodes. The vertex point symbols are $\{6^6.8^{14}.10^7.12\}$, $\{6\}$, $\{8\}$ and $\{6\}$ for the 8-connected SBU nodes and three kinds of 2-connected benzene nodes respectively. Therefore, the overall structure of 4 can be simplified to a 2,2,2,8-c 4-nodal topological network with point symbol of $\{6^6.8^{14}.10^7.12\}\{6\}_3\{8\}$.



Scheme 2. The coordination fashions of BDC^{2-} ligands in compound 4.

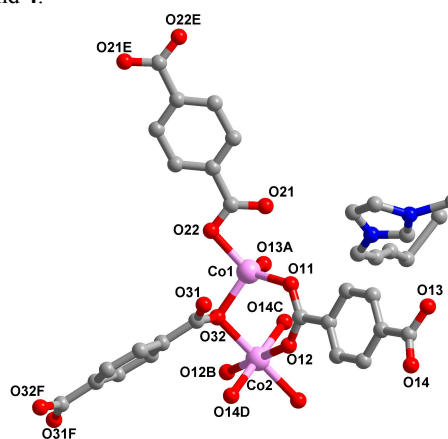


Figure 4. Coordination spheres of Co(II) centers in compound 4.



Figure 5. The structure motif of the linear trinuclear $[\text{Co}_3(\text{COO})_8]$ SBU in compound 4.

Compounds 1-3 can be obtained at 140 and 160 °C with the different molar ratios of H_2BDC ligands and Co^{2+} centers, suggesting the ligand configuration is the critical factor to determine the MOF structures, not the reaction temperature and the ratio. It demonstrates that the design of choosing simple ligand to eliminate the influence of the structure is effective. It is noteworthy that compounds 1-3 have the same general chemical formula $[\text{RMI}]_2[\text{Co}_3(\text{BDC})_3\text{Br}_2]$, and the same skeleton frameworks with $[\text{RMI}]^+$ cations locating in the interlayer space.

There are a lot of same structural details in **1-3**, such as the coordination fashions and the deprotonated degree of BDC²⁻ ligand, the coordination spheres of Co(II) centers, and the construction modes of the SBUs and the 2D skeletons.

Compound **4** also contains almost identical 2D grid as those in compounds **1-3** if omitting the difference in monodentate coordinated COO⁻ or Br⁻. Nevertheless, the subtle effect of [RMI]⁺ templates on the 2D rigid [Co₃(BDC)₃Br₂] skeletons still can be observed (Figure 6). (i) Under fixed almost all reaction conditions, such as the types of the starting materials and their molar ratios, the temperatures, and the anions of ILs, except only the different [RMI]⁺ cations in ILs, we obtained two types of MOF skeletons. Compared the skeleton frameworks of compounds **1-3** and **4**, the 2D (3,6) grid in compound **4** can grow into a 3D architecture with the connections of the BDC²⁻ ligands. The cause of this change may come from the sizes of [RMI]⁺ templates: [AMI]⁺ template has the top size in the presented [RMI]⁺ series, making the maximum interlamellar spacing (the interlamellar spacing represented by the centroid distances between the neighboring linear trinuclear SBUs, 12.927 Å for **1**, 12.977 Å for **2**, 13.082 Å for **3**, 17.234 Å for **4**), thus permitting the entry of BDC²⁻ ligands to fabricate the 3D architecture; (ii) The interlayer [RMI]⁺ templates exert influence on the diagonal sizes of the quadrilateral grids. With the increasing of the lengths of the alkyl chains in [RMI]⁺ templates, the quadrilateral grids stretch along *b*-direction and compress along *c*-direction (9.39 × 18.82 Å² for **1**, 9.45 × 18.78 Å² for **2** and 9.75 × 18.51 Å² for **3**), which matches the order of the steric hindrances of the alkyl chains; (iii) the changes in the solvent-accessible volumes of compounds **1-3** also support the deduction: with the increasing of the alkyl lengths, the gradual fall of the solvent-accessible volumes can be watched (61.7 Å³, 2.9% for **1**, 43.2 Å³, 2.0% for **2**, 0 Å³, 0 % for **3**). The solvent-accessible volumes under omitting the [RMI]⁺ templates comply with the trends (954.5 Å³, 45.4% for **1**, 972.4 Å³, 45.8% for **2**, 1009.4 Å³, 46.5 % for **3**). Calculated the solvent-accessible volumes of 2D grid with/without [AMI]⁺ template in compound **4** under omitting the μ₂ bis-monodentate BDC²⁻ ligands, the solvent-accessible volumes respectively are 1915.0 Å³, 32.5 % with [AMI]⁺ and 3830.3.0 Å³, 64.9 % without [AMI]⁺, which supports our analysis.

Characterizations

PXRD. The experimental PXRD patterns for compounds **1-4** match well with those simulated from single crystal structure data (Supporting Information, Figure S9), indicating that compounds **1-4** were isolated as single crystal pure phases.

FT-IR spectra. The characteristic absorption peaks of the main functional groups for compounds **1-4** are listed in Supporting Information (Table S2). The asymmetric stretching vibrations ν_{as}(COO⁻) are observed in the rang 1508-1635 cm⁻¹ and symmetric stretching vibrations ν_s(COO⁻) in 1380-1504 cm⁻¹. The above stretchings are shifted to lower wave numbers, compared to the carbonyl frequencies of free H₂BDC ligand (ν_{C=O} = 1682 cm⁻¹). The difference Δ(ν_{as}(COO⁻)-ν_s(COO⁻)) were beyond 200 cm⁻¹, showing the coordinated carboxylate groups,²⁶ in accordance with the single crystal structural analysis. The peaks for **1-4** from 2925 to 2980 cm⁻¹ are from C-H stretching vibrations, the ones around 1160 cm⁻¹ assigned to N-C stretching

of the imidazolium ring, and the one at ca. 3100 cm⁻¹ related with C-H stretching of the imidazolium ring.

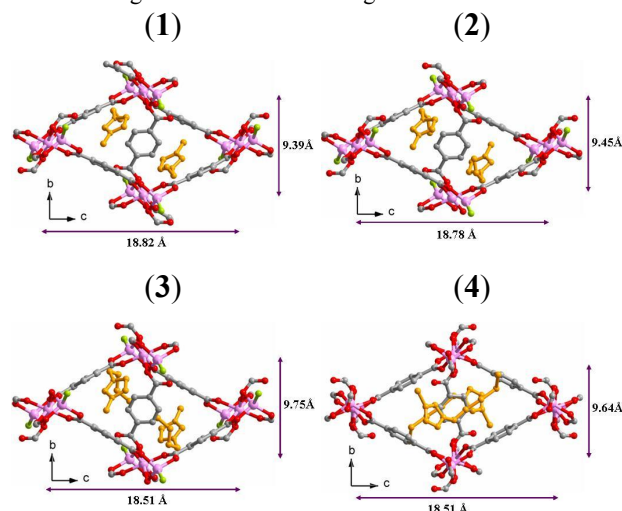


Figure 6. The sizes of the quadrilateral along with [RMI]⁺ in compounds **1-4**.

TG analysis. The thermogravimetric analyses of compounds **1-4** show their thermal stabilities up to around 400 °C for compounds **1-3** and 270 °C for compound **4**, and start to decompose at 410 for **1**, 402 for **2**, 388 for **3**, and 270 °C for **4** (Supporting Information, Figure. S10). The decreasing order of the thermal decomposition temperatures from **1** to **4** is contrary to that of the interlamellar spacing from **1** to **4**. This phenomena that less interlamellar spacing associates with higher thermal stability may suggest the effect of [RMI]⁺ cations on the structural stabilities. The very small weight loss of ca. 1.5% in **1** at 252°C may come from water absorbed by MOF or combining with [EMI]⁺ templates. In the following temperature range after the thermal decomposition temperatures, considerable weight losses (ca. 59.1-81.5%) occur, attribute to the destruction of the overall frameworks due to oxidation of the organic components including ILs and BDC²⁻ ligands. These losses with no plateau seem to concern with the decarboxylation and/or ring-opening reactions of the imidazolium ring. It also suggests [RMI]⁺ templates are very stable in the MOF frameworks, decomposing simultaneously with MOF skeletons, supporting the results that [RMI]⁺ templates can not be exchanged by common metal cations.

Fluorescence. The emission spectra of **1-4** and free H₂BDC ligand in the solid state are recorded at ambient temperature (Figure 7). Free H₂BDC ligand shows two emission peaks at 399 and 415 nm with the excitation at 330 nm, which can be assigned to π→π* and n→π* intraligand charge transfers (ILCT) respectively. Compounds **1-4** exhibit broad emissions at around 405 nm and shoulder peaks at around 465 nm (407 and 467 nm for **1**, 402 and 465 nm for **2**, 400 and 464 nm for **3**, and 410 and 466 nm for **4**) with the excitation at 350 nm. The neighbouring emissions of free H₂BDC ligand fuse into broad emissions at around 400 nm in compounds **1-4**. After the coordination of Co(II) center with H₂BDC ligand, a red shift and a blue shift occur at the π→π* and n→π* ILCT respectively, appearing as broad emissions. Compared to the free H₂BDC ligand, there are new emerging emissions at around 460 nm, which are assigned to

ligand-to-metal charge transfer (LMCT). By the observation on broad peaks at around 400 nm of **1-3**, we can find the wave lengths are blue shifting, whose order is contrary to the increasing alkyl chain in [RMI]⁺ templates. It hints the correlativity between the fluorescence and [RMI]⁺ templates that the longer the alkyl chain, the shorter the wavelength, relating with the solvent role of ILs.

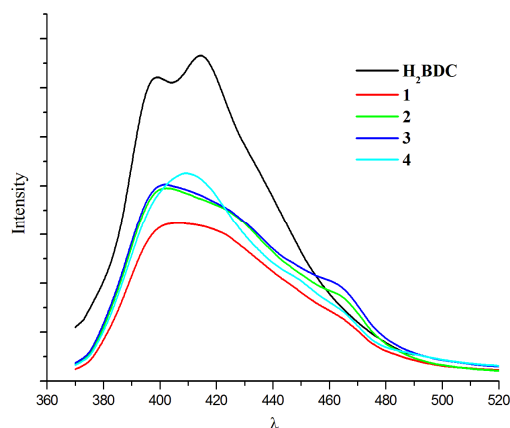


Figure 7. The solid-emission spectra of **1-4** ($\lambda_{\text{ex}} = 350$ nm) and H_2BDC ($\lambda_{\text{ex}} = 330$ nm) recorded at ambient temperature.

3	8.84777	0.34281	8.408
4	8.00311	12.13563	1.781

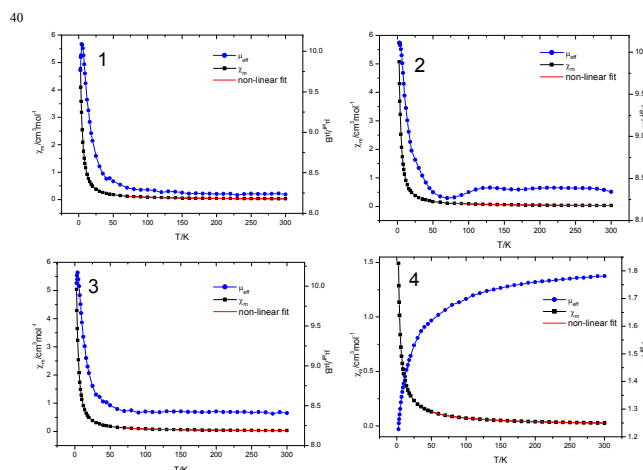


Figure 8. Plots of χ_m vs T and μ_{eff} vs T over 2-300 K at a field of 1000 Oe of compounds **1-4**.

Conclusions

In this present work, a series of Co-BDC metal-organic frameworks are synthesized by ionothermal method with four types of 1-alkyl-3-methyl imidazolium bromide [RMI]Br ILs. By fixing the factors, such as the types of the raw materials and their molar ratios, the temperatures, and the anions of ILs, we explored the effect of ILs on the structure constructions and the properties. Compounds **1-3** have the same (3,6) [$\text{Co}_3(\text{BDC})_3\text{Br}_2$] skeletons, and compound **4** distinguishes itself as a 3D architecture based on a almost identical 2D grid as those in **1-3**. By the comparison of the structures, the template role of [RMI]⁺ is clearly shown: [RMI]⁺ templates influence the diagonal sizes of the quadrilateral grids, the interlamellar spacing, and the solvent-accessible cavities through the steric hindrances. The decomposing temperatures of compound **1-3** around 400 °C and 270 °C for **4** show high thermal stabilities. The TGA of compound **1-3** indicate that their decomposing temperatures bear on the interlamellar spacing concerning with [RMI]⁺ sizes. Similar observation on their emission peaks at around 400 nm of **1-3** suggests the alkyl chain in [RMI]⁺ templates slightly affect the fluorescence. The magnetic behaviors of compounds **1-3** are similar ferromagnetism with close magnetic parameters, while compound **4** reveals an antiferromagnetic interaction. Our present work demonstrates that [RMI]⁺ templates exert significant influence on the structure construction and the properties through the alkyl chain length. It also proves the feasibility to tune the MOF structures and properties through tailoring the structures of the ILs components. Further investigation on such systems may give out more information derived from more new MOF materials with interesting features and desired properties.

Acknowledgment

This work was supported by the National Natural Science Foundation of China (21401122), the Fundamental Research Funds for the Central Universities (GK201402052), and Shaanxi University of Sciences and Technology (BJ14-02)

Magnetic properties. The crystal samples of compounds **1-4** were measured in the temperature range 2-300 K with magnetic fields of 1000 Oe, whose magnetic behaviors are shown in Figure 8 in the form of χ_m - T and μ_{eff} - T plots. Nonlinear fitting method via $\chi_m = C/(T - \theta)$ applied to the data of **1-4** between 50-300 K reveals the Curie-Weiss behaviors with the Curie constants and the Weiss constants. The effective magnetic moments of compounds **1-4** can be calculated via $\mu_{\text{eff}} = 2.828 (\chi_m T)^{1/2} \mu_B$ (Table 2). The effective magnetic moments μ_{eff} observed in compound **1-3** are much higher than the theoretical value (3.87 μ_B) of one magnetically isolated spin-only Co (II) ions ($l = 3$, $S = 3/2$, $g = 2.0$). The μ_{eff} - T plots show gradual increasing with the temperature decreasing, indicating the presence of ferromagnetic interactions. The results are well fitted by the Curie-Weiss law $\chi_m = C/(T - \theta)$ with positive θ values, and supported by the comparisons that average μ_{eff} values at around 8.3 μ_B (8.205 μ_B for **1**, 8.377 μ_B for **2**, 8.412 μ_B for **3**) are much larger than theoretical value (3.87 μ_B). The similar magnetic behaviors with close values of compounds **1-3** originate from the structure similarities. However, compound **4** shows an antiferromagnetic interaction judged by its μ_{eff} increasing depending on temperature, also supported by its negative θ ($\theta = -12.13563$ K) and μ_{eff} of 1.78 μ_B at ambient temperature less than theoretical value (3.87 μ_B).

Table 2. The Curie constants, the Weiss constants and the effective magnetic moments of compounds **1-4** via nonlinear fitting method

Compound	Curie constant C ($\text{cm}^3\text{mol}^{-1}\text{K}$)	the Weiss constant θ (K)	μ_{eff} at 300K (μ_B)
1	8.41854	1.82924	8.232
2	8.77425	0.02223	8.343

Notes and references

- ^a Key Laboratory of Macromolecular Science of Shaanxi Province, School of Chemistry & Chemical Engineering, Shaanxi Normal University, Xi'an, 710062, Shaanxi Province, P. R. China. E-mail: xuling@snnu.edu.cn (L.X)
- ^b College of Chemistry and Chemical Engineering, Shaanxi University of Sciences and Technology, Xi'an, 710021, Shaanxi Province, P. R. China.
- ^c REQUIMTE, Departamento de Química e Bioquímica, Faculdade de Ciências, Universidade do Porto, 4169-007 Porto, Portugal. E-mail: l.cunha.silva@fc.up.pt (L. C.-S.)
- Electronic Supplementary Information (ESI) available: TG graphs and observed and calculated XRPD patterns for compounds 1-4. Coordination sphere of Co in compound 2 and 3. The final 2D (3,6) layer (c) in compound 1-3 The 3D framework in compound 4 The main IR characteristic absorption peaks for compounds 1-4. See DOI: 10.1039/b000000x/
- P. Wassweachid and W. Keim, *Angew. Chem. Int. Ed.*, 2000, **39**, 3772.
 - E. R. Copper, C. D. Andrew, P. S. Wheatley, P. B. Webb, P. Wormald and R. E. Morris, *Nature*, 2004, **430**, 1012.
 - E. R. Parnham, P. S. Wheatley and R. E. Morris, *Chem. Commun.*, 2006, 380; E. R. Parnham and R. E. Morris, *J. Am. Chem. Soc.*, 2006, **128**, 2204; Y. P. Xu, Z. J. Tian, S. J. Wang, Y. Hu, L. Wang, B. C. Wang, Y. C. Ma, L. Hou, J. Y. Yu and L. W. Lin, *Angew. Chem. Int. Ed.*, 2006, **45**, 3965.
 - Z. Lin, D. S. Wragg and R. E. Morris, *Chem. Commun.*, 2006, 2021–2023; Z. Lin, D. S. Wragg, J. E. Warren and R. E. Morris, *J. Am. Chem. Soc.*, 2007, **129**, 10334; Z. Lin, Y. Li, A. M. Z. Slawin and R. E. Morris, *Dalton Trans.*, 2008, 3989.
 - R. D. Rogers and K. R. Seddon, *Science*, 2003, **302**, 792; Q. H. Zhang, K. De Oliveira Vigier, S. Royer and F. Jérôme, *Chem. Soc. Rev.*, 2012, **41**, 7108.
 - K. E. Gutowski, G. A. Broker, H. D. Willauer, J. G. Huddleston, R. P. Swatloski, J. D. Holbrey and R. D. Rogers, *J. Am. Chem. Soc.*, 2003, **125**, 6632. D. Camper, P. Scovazzo, C. Koval and R. Noble, *Ind. Eng. Chem. Res.*, 2004, **43**, 3049.
 - J. Hoffmann, M. Nuchter, B. Ondruschka and P. Wasserscheid, *Green Chem.*, 2003, **5**, 296; D. Freudenmann, S. Wolf, M. Wolff and C. Feldmann, *Angew. Chem. Int. Ed.*, 2011, **50**, 11050.
 - E. R. Parnham and R. E. Morris, *J. Mater. Chem.*, 2006, **16**, 3682.
 - X. J. Meng and F. S. Xiao, *Chem. Rev.*, 2014, **114**, 1522. (b) N. A. Khan, Z. Hasan and S. H. Jung, *Chem. Eur. J.*, 2014, **20**, 376.
 - B. Chen, X. Zhao, A. Putkham, K. Hong, E. B. Lobkovsky, E. J. Hurtado, A. J. Fletcher and K. M. Thomas, *J. Am. Chem. Soc.*, 2008, **130**, 6411; H. Furukawa, K. E. Cordova, M. O'Keefe and O. M. Yaghi, *Science*, 2013, **341**, 6149; X. Q. Kong, H. X. Deng, F. Y. Yan, J. Kim, J. A. Swisher, B. Smit, O. M. Yaghi and J. A. Reimer, *Science*, 2013, **341**, 882.
 - H. C. Zhou, J. R. Long and O. M. Yaghi, *Chem. Rev.*, 2012, **112**, 673; H. Furukawa, N. Ko, Y. B. Go, N. Aratani, S. B. Choi, E. Choi, A. O. Yazaydin, R. Q. Snurr, M. O'Keefe, J. Kim and O. M. Yaghi, *Science*, 2010, **329**, 324.
 - K. Jin, X. Huang, L. Pang, J. Li, A. Appel and S. Wherland, *Chem. Commun.*, 2002, 2872; D. N. Dybtsev, H. Chun and K. Kim, *Chem. Commun.*, 2004, 1594; W. Wang, Y. Li, L. Liu and J. X. Dong, *Dalton Trans.*, 2012, **41**, 10511; Z. Jiang, G. Y. Jiang, D. C. Hou, F. Wang, Z. Zhao and J. Zhang, *CrystEngComm.*, 2013, **15**, 315.
 - Z. C. Zhao, W. P. Zhang, R. S. Xu, X. W. Han, Z. J. Tian and X. H. Bao, *Dalton Trans.*, 2012, **41**, 990; Q. Y. Liu, Y. L. Wang, N. Zhang, Y. L. Jiang, J. J. Wei and F. Luo, *Cryst. Grow. & Des.*, 2011, **11**, 3717; B. Tan, Z. L. Xie, M. L. Feng, B. Hu, Z. F. Wu and X. Y. Huang, *Dalton Trans.*, 2012, **41**, 10576; W. X. Chen, G. L. Zhuang, H. X. Zhao, L. S. Long, R. B. Huang and L. S. Zheng, *Dalton Trans.*, 2011, **40**, 10237; D. Carriazo, M. C. Serrano, M. C. Gutiérrez, M. L. Ferrer and F. del Monte, *Chem. Soc. Rev.*, 2012, **41**, 4996; J. H. Qin, Y. Y. Jia, H. J. Li, B. Zhao, D. Q. Wu, S. Q. Zang, H. W. Hou and Y. T. Fan, *Inorg. Chem.*, 2014, **53**, 685.
 - L. Liu, D. B. Luo, D. F. Li and Z. Lin, *Dalton trans.*, 2014, **43**, 7695; Z. G. Jiang, K. Shi, Y. M. Lin and Q. M. Wang, *Chem. Commun.*, 2014, **50**, 2353; Q. Y. Liu, Y. L. Li, Y. L. Wang, C. M. Liu, L. W. Ding and Y. Liu, *CrystEngComm.*, 2014, **16**, 486; T. G. Parker, J. N. Cross, M. J. Polinski, J. Lin and T. E. Albrecht-Schmitt, *Cryst. Grow. & Des.*, 2014, **14**, 228; C. Y. Yue, X. W. Lei, Y. X. Ma, N. Sheng, Y. D. Yang, G. D. Liu and X. R. Zhai, *Cryst. Grow. & Des.*, 2014, **14**, 101.
 - L. Xu, E.-Y. Choi and Y.-U. Kwon, *Inorg. Chem.*, 2007, **46**, 10670; L. Xu, E.-Y. Choi and Y.-U. Kwon, *Inorg. Chem.*, 2008, **47**, 1907; L. Xu, S. H. Yan, E.-Y. Choi, J.-Y. Lee and Y.-U. Kwon, *Chem. Commun.*, 2009, 3431; L. Xu, Y.-U. Kwon, B. de Castro and L. Cunha-Silva, *Cryst. Grow. & Des.*, 2013, **13**, 1260.
 - E. R. Parnham and R. E. Morris, *Chem. Mater.*, 2006, **18**, 4882; P. Bonhote, A. P. Dias, N. Papageorgiou, K. Kalyanasundaram and M. Cratzel, *Inorg. Chem.*, 1996, **35**, 1168.
 - A. F. Wells, *Three-Dimensional Nets and Polyhedra*, Wiley-Interscience, New York, 1977.
 - V. A. Blatov, Multipurpose crystallochemical analysis with the program package TOPOS, IUCr CompComm Newsletter, 2006, **7**, 4; <http://www.topos.ssu.samara.ru>.
 - T. Kottke and D. Stalke, *J. Appl. Crystallogr.*, 1993, **26**, 615.
 - APEX2, Data Collection Software Version 2.1-RC13, Bruker AXS, Delft, The Netherlands 2006.
 - Cryopad, Remote monitoring and control, Version 1.451, Oxford Cryosystems, Oxford, United Kingdom 2006.
 - SAINT+ , Data Integration Engine v. 7.23a © 1997–2005, Bruker AXS, Madison, Wisconsin, USA.
 - G. M. Sheldrick, SADABS v.2.01, Bruker/Siemens Area Detector Absorption Correction Program 1998, Bruker AXS, Madison, Wisconsin, USA.
 - Siemens, SHELXTLTM Version 5 Reference Manual 1994, Siemens Energy & Automation Inc., Madison, Wisconsin, USA.
 - A.L. Spek, *Acta Crystallogr.*, 1990, **A46**, C34.
 - K. Nakamoto, *Infrared Spectra of Inorganic and Coordination Compounds*, Wiley, New York, 1986; G. B. Deacon and R. Philips, *J. Coord. Chem. Rev.*, 1980, **33**, 227; C. Djordjevic and M. Lee, E. Sinn, *Inorg. Chem.*, 1989, **28**, 719.